A calibration set for ocular aberrometers: Manufacture, testing and application

Pablo Rodríguez, MS [1,2], Rafael Navarro, PhD [1,2], Justo Arines, MS, OD [3], Salvador Bará, PhD [3]

1.- Instituto de Óptica "Daza de Valdés", CSIC
2.- Departamento de Física Aplicada. Universidad de Zaragoza
3.- Área de Óptica. Universidade de Santiago de Compostela, Galicia.

Corresponding author:

Pablo Rodríguez
Departamento de Física Aplicada
Universidad de Zaragoza
50009 Zaragoza
Spain

Phone: (34) 976 761000
Fax: (34) 976 761233
E-mail: prodrigp@unizar.es

Number of words: 5915

Concerning the research or instruments described in this article, the authors Pablo Rodríguez, Rafael Navarro, Justo Arines and Salvador Bará hold patent rights on the set of phase plates for the calibration of aberrometers.

ABSTRACT:

Purpose. To manufacture and test a set of phase plates for the calibration of ocular aberrometers and eventually to apply it to the calibration of an ocular laser ray tracing aberrometer.

Methods. The set of phase plates is made by a grey-scale single-mask photosculpture in photoresist method. Each plate induces a given amount of a particular aberration (Zernike) mode. The set contains two subsets: (1) different pure Zernike modes to test the accuracy among different orders (from 3^{rd} to 7^{th}, about 0.3 - 0.4 microns); and (2) plates having different amounts of the same mode, 3^{rd} order coma ranging from 0.11 to 0.47 microns. Right after manufacturing, the plates were tested twice, as a cross-check, measuring the aberration pattern of each plate with a Mach-Zehnder interferometer and a single-pass Hartmann-Shack wavefront sensor. The set was then applied to the calibration of an ocular double-pass laser ray tracing aberrometer.

Results. We found a close agreement between the three types of measurement. The maximum difference between H-S and LRT measurements was 0.032 μm (that is about λ/20, half of the typical measuring error in human eyes). This permitted us to detect a small bias in the ocular laser ray tracing aberrometer.

Conclusions. The calibration set may be a powerful tool for the assessment of accuracy and reliability in ocular aberrometry. It allowed us to discover a small bias, that is almost impossible to detect working with human eyes or trial lenses. This type of calibration tool is especially important in clinical environments.

1. INTRODUCTION

Aberrometry is a widely used method to assess the optical quality of the eye. It has quickly evolved from an experimental technique into a common clinical tool. In particular, it is becoming essential in refractive surgery or in the field of advanced retinal imaging. Different types of experimental ocular aberrometers have been reported in the literature, for example the Hartmann-Shack wavefront sensor (H-S)[1], the Laser Ray Tracing (LRT)[2], the Tscherning type[3], or psychophysical methods[4,5], and for most of them there are commercially available systems. The performance of several of these aberrometers has been studied in laboratory prototypes and their reliability has been demonstrated also through cross-validation in both artificial and real eyes[6,7,8,9,10], and even through direct comparison between commercial and experimental devices[11]. Nevertheless, most of these studies are focused on the repeatability or equivalence of the devices, but leave aside their accuracy, in part due to the lack of appropriate, easy-to-use aberration generators (aberrators). The accuracy of aberrometers has been mainly assessed by means of trial lenses, which induced variable amounts of defocus and astigmatism, that is, only second order aberrations, in artificial eyes. However, the main application of aberrometry is to measure higher order aberrations (HOA), and hence it seems necessary to assess the accuracy in HOA measurements. This is even more important in clinical environments, where ocular aberrometers should undergo frequent calibration and maintenance operations in order to ensure a completely reliable performance of these precision instruments.

Several devices have been developed to generate controlled wavefront aberrations. Deformable mirrors (DM) and liquid-crystal spatial light modulators (LC-SLM) have been used to this end[12,13], but their real applicability for calibration of ocular aberrometers is limited by their high cost and low portability. Aspherical lenses have also been proposed to correct or induce specific aberration modes (i.e. spherical and coma), but they are limited to these particular cases[14].

Here, we present a set of phase plates, in which each plate induces a given amount of a particular aberration (Zernike) mode. The reason for using single-mode plates is double: On the one hand it

allows us to simplify the problem of sampling the n-dimensional space of all possible wavefront aberrations, and what is more important, single modes have the important property of being basically insensitive to lateral misalignments, which guarantees the robustness of calibrations[15]. We have included two main subsets of plates, one has one sample per Zernike order, and the other samples the scale (amount) of aberrations. In addition, a couple of plates have been duplicated to include some redundancy in the testing, and also to check the repeatability of our manufacture processing. The phase plates are made by a grey-scale single-mask photosculpture in photoresist method[16,17], which had already been successfully applied to manufacture plates with continuous refractive profiles for the static correction of ocular aberrations[18]. It has the advantages of a high spatial resolution, that permits the generation of even very high order Zernike modes with high fidelity, and relatively low cost.

In what follows we present, first the design and manufacture of the phase plates. The optical testing and characterization consisted of a double calibration and cross-check of the manufactured plates by both a Mach-Zehnder interferometer and a single-pass Hartmann-Shack wavefront sensor. Finally, the set is applied to test a double-pass ocular laser ray tracing (LRT) experimental aberrometer[2]. It is shown how the use of this calibration set enabled us even to find a little bug in the aberrometer control software, which caused a rather small difference in the pupil sampling between the X and Y directions.

2. MATERIALS AND METHODS

The complete experimental procedure consists of two main parts. The first stage is to obtain the calibration set ready, which includes design, manufacture, double testing and characterization; the second stage is the application to the testing, calibration and fine-tuning of an ocular LRT experimental aberrometer. It is worth mentioning that most of the experimental work corresponding to these two stages has been done independently in two different laboratories. Most of the

manufacture and testing of the calibration set has been done at the University of Santiago de Compostela, while most of the design and application has been done independently at the CSIC-University of Zaragoza joint laboratory.

2.1 Design

The calibration set consists of a series of phase plates, each producing a given amount of a pure Zernike mode aberration, typically measured in microns root-mean-square (RMS). We have excluded second order aberrations (defocus and astigmatism) and considered only higher order aberrations (HOA). Aberrometers should ideally behave consistently and linearly both across magnitude of aberrations, and across modes of aberration. Thus a calibration set should contain samples of different modes, and samples with different magnitudes. Multimode aberration patterns, such as examples of complex aberration patterns measured in real eyes, are excluded from the calibration set, because they require an extremely accurate positioning and alignment of the plate. Even small decentrations tend to cause a drastic redistribution of magnitudes among the modes[15,19]. Here we considered the fact that monomode aberration patterns, on the contrary, have the nice theoretical property of translation invariance: Misalignments only introduce additional lower order modes, without changing the value of the nominal mode[15]. Thus mono-mode plates seem especially appropriated, their use being much simpler and providing a much higher robustness in calibration applications. Nevertheless, it is important to bear in mind that, in practice, this theoretical property holds as long as the manufactured phase plates show negligible high order residual aberrations.

After these considerations, we have taken samples along the two main variables (mode and magnitude) and therefore obtained two different calibration subsets. Figure 1 shows the wavefront aberration maps and theoretical interferograms corresponding to each plate of the two calibration subsets. The intensity at a point of the interferogram is proportional to the cosine of the phase change induced by the plate, so that an odd-symmetric aberration pattern (e.g. coma) produces an even-symmetric interferogram. In the first subset we have included one plate per Zernike radial

order, from 3rd to 7th. This almost covers the whole range of significant aberrations found in normal, healthy eyes[20]. In order to also include a variety of angular symmetries, we have chosen (see Fig. 1) the modes Z_3^{-3}, Z_4^{-2}, Z_5^{-1}, Z_6^{2} and Z_7^{5}, following the notation recommended by the Optical Society of America[21]. The second variable, magnitude, is doubly sampled by assigning different amounts to the first subset and by including a second specific subset, in which all the plates produce the same mode of aberration (Z_3^{1}, coma) but in a different amount (see Fig. 1). We have chosen this low order aberration, because it is well-known[20] that, in the eye, the magnitude of aberrations rapidly decreases with order, and therefore the lower orders have the higher values. In this subset we have considered four different values, but included a second copy of two of the plates (Z_3^{1} (1) and Z_3^{1} (2)) to check the repeatability in the manufacture process, and also because it could be convenient to include some double (redundant) samples in the calibration set.

The phase plates work by inducing optical path differences, *OPD*, by local differences in thickness. The *OPD* between rays passing at different locations is:

$$OPD = (n' - 1)\Delta z \qquad (1)$$

where n' is the refractive index of the plate and Δz is the difference in thickness along the direction of propagation of the light (optical axis of the aberrometer). It is important to note that the materials (photoresist in our case) show chromatic dispersion, that is n' changes with wavelength, and so does the aberration induced by the plate. The chromatic dispersion curve of the photoresist, provided by the manufacturer, is such that the refractive indexes at the wavelengths more commonly used in aberrometers is n'(532nm)=1.6602, n'(632nm)=1.6406 and n'(780nm)=1.6245. Therefore, the OPD slightly changes with wavelength, being about 64% of the photoresist thickness for red light. With the parameters used in our present procedures, layer thicknesses up to ten microns may be attained, which allow to generate OPD up to 6.4 microns. For other wavelengths, we have to apply a correction factor that is 1.03 for green and about 0.975 for near infrared. This factor has to be taken into account when using the phase plates for calibration at different wavelengths. All the results

reported below are normalized in this way, and are given for the reference wavelength of 632.8 nm, that is the one used in the interferometric testing.

The size of the plates is scaled to typical aberrometric measurements in the eye. Here we have considered a standard diameter of 6.40 mm for all the plates in the set.

2.2 Manufacture

The manufacture process of the phase plates has been described before[18]. It is based on a grey-level single-mask photosculpture in photoresist technique, implemented at the University of Santiago de Compostela. We start with a flat plate that is a cleaned soda lime glass substrate spin coated with Shipley S1828 positive photoresist at 1000 to 1500 rpm during 30 s and prebaked at 90 ºC for 30 min to evaporate the solvent. In this way we obtain a solid photoresist layer that is 5 to 6 μm thick. This thickness is representative of the typical layers than can be obtained with this photoresist, although values up to ten microns can be achieved by tuning the coating parameters. Other photoresist compositions can be used for obtaining even thicker layers, if it were found necessary for generating higher amounts of aberration. The maximum achievable thickness of a photoresist layer depends on the mechanical properties of the photoresist and on the coating procedure: spin coating at low speeds allows for thicker layers, but too low speeds may give rise to undesired thickness non-uniformities. Once coated, the plate is exposed to ultraviolet radiation, through a variable-transmittance mask that encodes the desired phase. After development, the variable-irradiance dose absorbed by the photoactive compound gives rise to a three-dimensional continuous profile of unequal depth. By a careful calibration of the entire process, which has shown a reasonably good linearity, it is possible to obtain a good match between the nominal (design) and final (real) profile. Nevertheless, this is a complex procedure, and it is important to perform a final testing and characterization of the manufactured plates, especially if they are going to be used as calibration tools.

2.3 Testing

The aberration pattern produced by each plate was characterized and tested by both interferometric and aberrometric measurements. A Mach-Zehnder interferometer working at 632.8 nm was used to carry out the first test. The interferograms were imaged on a CCD camera, trying that the intensities were within the linear range of the camera's response. Several interferograms were taken per plate, shifting the phase of the reference wave (piston) to check for the consistency of the results. The intensities of the test and reference channels and the fringes obtained without phase plate were recorded too. For most plates we had 3 or more interferograms, except for a couple of coma plates for which we only got one interferogram. As an additional test, the point-spread functions (PSF) of the phase plates were also recorded by means of a 25mm focal lens (see Fig. 2)**.**

A specific algorithm was developed to analyse the interferograms. The algorithm takes the advantage that the phase plates contain a known single Zernike mode. Under this strong simplification we perform a non-linear least squares fit of the theoretical interferogram to the experimental one, where the free parameter is the RMS value, in microns, of the Zernike mode. In practice, we have to consider that the interferogram also contains piston (relative phase of the reference) and tilt (residual alignment errors), thus we have 4 free parameters to fit (piston, X and Y tilts, and the plate mode). Therefore, in this fitting, we consider that the interferometer does not introduce additional aberrations, except tilts and piston terms, thus neglecting other potential residual phase. Nevertheless, as a control measure, phase errors introduced by potential defects in the interferometer were estimated from reference interferograms recorded without phase plate, being lower enough for not affecting the measurement of the plate mode (0.012 μm RMS). A typical drawback of non-linear fitting is that the input guess must be close to the real value to guarantee convergence to the minimum. Therefore we used the nominal value of the mode as input guess, which was close enough in most cases. Eventually we analysed the resulting fitting error to estimate confidence limits (see Discussion Section). This fitting method has performed quite well

for higher order modes, but we have experienced a lower performance for the coma (third order) plates. For these lower order plates, the algorithm was less robust and occasionally it did not converge properly. The origin of this behaviour could be related to a coupling between the tilt and coma terms, as shown by the rather high residual tilts obtained for these interferograms. For this reason, we had to discard several interferograms for the coma plates.

This algorithm does not provide a complete fringe analysis of the interferograms. It permits us to calibrate the value of the main mode of the plate, but this characterization is not totally complete, because the resultant phase plates are not pure mono-mode since they usually have other residual aberrations due to manufacture errors. The presence of these residual modes may be detected through the fitting error of the interferograms. This residual fitting error is a rough estimate of the rest of Zernike modes, not included in the fitting. It is possible to quantify the magnitudes of each of the residual modes from the interferograms, either by a second numerical adjustment of the residual fitting error, or by other alternative fringe analysis algorithms. Nevertheless, we have measured them directly with a single-pass Hartmann-Shack wavefront sensor for optical testing. The Hartmann-Shack measurements are used as a cross validation of the main mode of the plate, and additionally, to measure the magnitudes of each of the residual Zernike modes.

A single-pass Hartmann-Shack wavefront sensor was built at the University of Santiago de Compostela. It uses a square 11x11 lenslet array, each with 49.6 mm focal length and 564 microns diameter; the light source was a yellow LED (590 nm). This partially coherent source has the advantage of minimizing speckle noise that is one of the most important sources of variability in this kind of measurements. The phase plate is inserted at a plane conjugated with the lenslet array, and a CCD camera takes 30 short exposure images that are averaged to obtain a single H-S spot diagram image. For the 6.40 mm diameter of the plates, the number of spots in the H-S pattern is 89. The image was analysed in the standard way to compute the set of centroids of the spots, and

from them, the values of the modes. We used a Zernike polynomial expansion up to 7th order, which is the range covered by our phase plates set.

2.4 Application: Calibration of Laser Ray Tracing ocular aberrometer

The calibration set was then used to test an experimental laser ray tracing (LRT) ocular aberrometer developed at the Joint Research Unit CSIC-University of Zaragoza. On the contrary to the single-pass aberrometers used in optical testing[22], ocular aberrometers work in a rather different way, since in the eye we cannot place a camera in the image plane, and hence they work in a double-pass configuration[7]. This introduces additional sources of noise (speckle, etc.) and variability in the measurements, causing a rather modest signal-to-noise ratio[11], lower than in single-pass systems. The LRT ocular aberrometer has been described in detail before[2,22]. This system delivers, sequentially, a bundle of laser pencils (rays) and the corresponding retinal spot formed by each ray is imaged onto a CCD camera. This system has a high flexibility, and we have a complete freedom to program, in real time, the type of sampling pattern, pupil diameter, etc. In addition, we can use different wavelengths. The current version supports two lasers (usually green and infrared) simultaneously, although typically we only use one at once. The system also includes a second digital camera for pupil monitoring. The camera works in continuous grabbing mode when aligning the subject's eye, but during the ray tracing, it takes a snapshot per ray, synchronised with the retinal camera, thus recording both the pupil position and the intercepts of the laser beams with the cornea. These images are analysed to compensate for potential pupil misalignments during the measurements. In this case, we will be measuring a static artificial eye, so that we only need to analyse one of these pupil images to check the pupil alignment.

In the present experiment the working wavelength was 532 nm, and the number of rays (spots) sampling the 6.40 mm diameter of the plates was 89 in a square grid, to reproduce the sampling pattern of the single-pass H-S wavefront sensor exactly. With the current setup, one measurement

run takes about 1.5 seconds, since the ray tracing speed is 60 Hz, that is limited by the current hardware (cameras and data bus).

The plates are inserted as close as possible to the pupil plane of an artificial eye[7] consisting of a 200 mm lens doublet corrected for spherical aberration, and a rotating white screen that acts as "artificial retina". Small axial displacements between the plates and the eye's pupil have been shown, both experimentally[18] and theoretically[19], to have a rather small effect on the aberration pattern produced by the plate. In any case, the actual aberration at the pupil can be computed using a forward-propagation method such as that described in Ref.19. In our experiment, this small displacement did not introduce a noticeable bias.

The linearity and accuracy of the LRT system had been verified previously for second order aberrations using a set of trial lenses inserted in the artificial eye. For defocus and astigmatism terms, the linearity was extremely high, while the maximum differences between measured and nominal diopters of the trial lenses were less or equal to 3%.

Since one of the most useful potential applications of the phase plates is fine tuning of aberrometers, we thought that it would be especially interesting to study potential little biases due to residual errors in the LRT setup. Results of these tests are given in the discussion Section.

3. RESULTS

Figure 3 shows the wave aberration generated by the set of phase plates, measured by the different methods and aberrometers. The first column displays the recorded raw interferograms, while the other three columns display simulated interferograms computed from the Zernike coefficients: The second column shows the result of the non linear least squares fit of the raw interferograms; the third column corresponds to the wave aberrations measured with the single-pass Hartmann-Shack wavefront sensor; and the last column displays the result of the calibration of the LRT ocular aberrometer. To facilitate the visual comparison between the raw interferograms and the computed

ones, we have added the piston and tilt terms, measured on the interferograms of the first column, to compute the wavefronts displayed in the other three columns. In addition, the image intensity of the computed interferograms (columns 2, 3 and 4) has been normalized to the mean intensity of the raw interferograms (first column).

As we can see, all the interferograms show a high degree of resemblance, although several small differences can be appreciated. In particular, small displacements and in-plane rotations can be observed in the aberrometric measurements, mainly in the LRT calibration (see for instance plate Z_3^1 (3)). This kind of small misalignments and rotations has to be expected in real applications, but as we discuss below, single-mode plates are especially robust to these potential errors.

Quantitative results are given in Figure 4. The upper panel displays the nominal and measured values of the principal Zernike mode, RMS in microns, of each plate in the calibration set. The white bars correspond to the design target value, and the rest of bars to the different measurements: fitted Mach-Zehnder interferograms (grey bars), single-pass H-S (black) and two ocular LRT series of measurements (slashed and dotted bars). The lower panel shows the residual RMS aberration corresponding to all the modes, except the nominal one, for each plate, for the aberrometric measurements. The design target values, used as input to the manufacturing procedure, are in general slightly higher than the values actually obtained. This bias is small for lower order aberrations and appears to increase gradually with the Zernike radial order. The differences range from 0.8% (0.004 μm for plate Z_3^1 (4)) up to 16.6% (0.057 μm for plate Z_6^2), average 8.5% (0.025 μm). In other words, the manufacture process is not exact, which has two effects: differences between nominal and measured values and the presence of other residual aberration modes. In particular, the fact that measured values are lower than nominal ones indicates that in this batch the development time was slightly higher than optimum. Nevertheless, the accuracy of the manufacturing process is independent of the accuracy attainable in the calibrations made with the plates, which basically depends on their proper characterization.

We can see that, in general, there is a close agreement between the three types of measurement, M-Z, H-S and unbiased LRT (we will discuss the biased LRT below). The M-Z fitting algorithm tends to give slightly higher values. This bias is more marked for the interferograms of some of the coma plates, mainly Z_3^1 (2B) and Z_3^1 (3). The reason was that most of the interferograms obtained with these plates had to be discarded, because the fitting algorithm did not converge properly, and even the resulting fitting errors for the remaining interferograms were still high, and hence the results are less reliable for these plates. In fact, we experienced that, in general, it was harder to apply the non linear fit to the Mach-Zehnder interferograms for the coma plates.

Apart from that, the results obtained with the three types of measurements are highly consistent. Concerning the reproducibility of the manufacture process, we found a close match between the two copies of the duplicated plates: Z_3^1 (1A) and (1B); Z_3^1 (2A) and (2B), even across devices. In fact, the maximum difference found between the H-S and LRT measurements for these plates is about 0.010 μm, roughly $\lambda/60$. These results confirm the high reproducibility of the photosculpture in photoresist manufacture method. However, this manufacture process introduces a significant amount of residual aberrations, in addition to the desired nominal Zernike mode, as shown in the lower panel of Fig. 4. The averaged RMS of the residual aberrations is 0.057 μm for the H-S measurements, which is relatively constant regardless of the mode number or the mode magnitude. However, if we compare these residual aberrations with those provided by the ocular LRT aberrometer (biased), we can see that for the latter (slashed bars) the residual aberration is significantly larger, especially for some plates, so that the average is 0.101 μm, that is almost double than for the H-S measurements. As discussed below, this result suggests the presence of some small, difficult-to-detect, error in the LRT system. In fact, once the error is localized and fixed, we obtain the unbiased results (dotted bars), which show a much closer agreement between the two aberrometric measurements.

It is worth mentioning that all the results include error bars, although they can be hardly be seen in aberrometric measurements. Both single-pass H-S and double-pass LRT with artificial eye provide a signal-to-noise ratio, SNR, much higher than typical values obtained in real eyes, especially for HOA[11]. The SNR is especially high for the single-pass H-S wavefront sensor that is totally free from speckle noise, since there is no "retinal" scattering and a partially coherent LED light source is used. By contrast, the fitting algorithm used with the interferograms provides a rather moderate SNR as compared to the aberrometric measurements. In general, a relatively high number of phase-shifted images are needed to obtain accurate results[23].

4. DISCUSSION

The results obtained so far suggest that it is possible to manufacture phase plates for a calibration set with high accuracy and reproducibility and at a relatively low marginal cost. Although the photosculpting technique involves many stages (some of them are non-linear processes), a careful handling can lead to a highly reliable outcome. The high spatial resolution achieved with this technique permits the generation of high order Zernike polynomial modes, which have shown to be especially helpful in order to detect even small errors and biases in ocular aberrometers. Even if the mechanical properties of photoresist do not make these elements particularly fit for frequent and direct use in clinical settings, photoresist plates can be used as masters for moulding polymers, transferring the photoresist profile to more suitable materials. Experimental work with this goal is presently being carried out at our laboratories. As in other aberration generators, the peak-to-valley wavefront error that can be generated by the plates is limited. However, the progress in microfabrication technology has lead to the development in recent years of new photoresist compositions that allow to produce layers with thicknesses in the range of several tens of microns, so this seems not to be a fundamental limitation for their application in visual science. In fact, most of the manufactured plates generate aberrations much higher than those found in normal eyes for

the same modes, especially for higher orders. In addition, it is possible to put several plates together to simulate highly aberrated eyes.

The calibration set only includes mono-mode plates to enhance robustness. As we said before, one critical issue in aberrometry is alignment[19]. In Figure 3, some LRT measurements show displacement and/or in-plane rotations, as it can be expected in real applications, where the specific plate holder and the skill of the experimenter to place and align the plates can vary from one place to another. As we have already stated, this potential problem is minimised by the use of mono-mode plates, for which the value of their nominal Zernike mode should remain basically invariant, provided that these positioning errors are not too large. In practice, however, the manufacture process makes that the phase plates are not exactly mono-mode. It also generates other residual aberrations (typically higher order), and hence they are not 100% invariant to misalignments. These residual errors are small compared to the mode of the plate in all cases (see Fig. 4), but they have some influence on the variability and accuracy of the results, in particular for the larger rotations and misalignments of some of the coma plates. Nevertheless, these in-plane rotations can be easily detected either visually or by analysing the Zernike coefficients: The rotation of a mode would generate the appearance of its angular symmetric mode (corresponding to reversing the sign of the Zernike upper index). We have verified that these rotations are easy to detect and correct numerically[15], so that the value of the principal mode remains practically unchanged even for relatively large rotations (less than 1% in the worst case). Anyway, these small residual errors due to rotations and displacements can explain the slightly higher residual aberration measured with the LRT ocular system, even after fixing the detected error (see Fig. 4b) as compared with the H-S sensor.

The Mach-Zehnder interferograms of the plates give useful information to guide the calibration process. They have a spatial resolution remarkably bigger than that of the aberrometers and thus carry information of all modes present in the wavefront, not just of the modes detected by the

aberrometers. They constitute an independent set of results against which to compare the interferograms computed from the phase estimations obtained with wavefront slope sensors as the H-S or LRT. A simple visual comparison of actual and computed interferograms often allows to detect at once whether some relevant displacement or rotation of the phase plate has happened between methods.

As we have mentioned before, as an illustrative example of the potential applications of the calibration set, it was possible for us to detect a rather small error in the LRT system by using the calibration set. It turned out to be a little bug in the control program which caused that the effective pupil measured by the system was not exactly circular but slightly elliptical, because the motion of the laser scanner was slightly different between the X and Y axes. The difference was so small that the maximum difference between H-S and LRT measurements was of only 0.032 μm (that is about λ/20), what is about half of the typical measuring error in human eyes[11]. Interestingly, this maximum difference was found for the higher order plates Z_6^2 and Z_7^5. A deeper analysis showed that, in fact, the difference between the two aberrometers tended to increase monotonically with the aberration order (see Fig. 4a), which suggested the presence of some systematic, although extremely small, bias. Intuitively, this kind of dependence upon the order of the Zernike radial order suggests some calibration error in the pupil radius. In the LRT setup, the pupil is sampled by means of a XY laser scanner[7]. Thus, we carefully checked whether the XY coordinates of the rays at the pupil plane were the same as the nominal values. For this purpose, a CCD camera was placed at the plane of the pupil to record the spots formed by the rays. The centroids of these spots were computed in the standard way to compare real and nominal pupil positions. In this way we found that the pupil sampling was actually slightly elliptical, since the displacements of the scanner in the Y axis were 5% shorter than in the X axis. A simple numerical analysis showed that this error could totally explain the differences between H-S and LRT of Figure 4.

Once this bug was fixed, the calibration was repeated obtaining the results shown in Figure 4 (dotted bars). There is a considerable improvement in both the residual RMS and the match between the two aberrometric methods. Only one plate $Z_3^1(4)$ still shows significantly different values between the two aberrometric measurements (and to a lower extent Z_3^{-3}). As we said before, larger differences were found between aberrometric and interferometric measurements, especially for coma plates. This is probably due to limitations of our interferogram fitting algorithm, which works better with higher orders, but has shown convergence instabilities with several of the interferograms of the coma plates. We have also experienced that interferograms are more affected by experimental noise, which affects the fitting algorithm. Thus they have the advantage of being a more complete test, but somewhat less robust to noise. This makes the results of the fitting algorithm less reliable in some cases. The aberrometric measurements are more robust, and the accuracy and reliability of our experimental aberrometers (both single-pass Hartmann-Shack for optical testing and double-pass ocular LRT) have been largely validated by the close agreement found. This is consistent with previous findings[7,10], but now, thanks to the use of the calibration set, we have significantly improved the accuracy, been able to demonstrate an even closer match.

In conclusion, the calibration set, that we have presented so far, may be a powerful tool for the assessment of accuracy and reliability in ocular aberrometry. It allowed us to discover a rather small bias, that is almost impossible to detect only working with human eyes, due to the high noise level, or even with other calibration tools, such as trial lenses (second order aberrations). In fact, the error detected with the calibration set produced a bias so small that was virtually undetectable for low aberration orders, and only comparing different radial orders could be detected. This type of calibration tool is especially important in clinical environments. Clinical aberrometers are often exposed to high levels of usage and thus to a greater risk of suffering some kind of alteration. A reliable calibration procedure should be frequently applied to these devices, whose measurements are sometimes used even to guide surgery techniques.

Acknowlegments

This work has been partially supported by the Comisión Interministerial de Ciencia y Tecnología (Spain), under grant DPI2002-04370-C02. Pablo Rodríguez acknowledges a grant from a collaboration program between the Secretaría de Estado de Universidades e Investigación del Ministerio de Educación y Ciencia and the Consejo Superior de Investigaciones Científicas.

REFERENCES

1.- Liang J, Grimm B, Goelz S, Bille JF. Objective measurement of wave aberrations of the human eye with the use of a Hartmann-Shack wave-front sensor. J Opt Soc Am A 1994;11:1949-1957.

2.- Navarro R, Losada MA. Aberrations and relative efficiency of light pencils in the living human eye. Optom Vis Sci 1997;74:540-547.

3.- Mierdel P, Krinke HE, Wiegand W, Kaemmerer M, Seiler T. Measuring device for determining monochromatic aberration of the human eye. Ophthalmologe 1997;94:441-445.

4.- Howland HC, Howland B. A subjective method for the measurement of monochromatic aberrations of the eye. J Opt Soc Am 1977;67:1508-1518.

5.- He JC, Marcos S, Webb RH, Burns SA. Measurement of the wave-front aberration of the eye by a fast psychophysical procedure. J Opt Soc Am A 1998;15:2449-2456.

6.- Prieto PM, Vargas-Martin F, Goelz S, Artal P. Analysis of the performance of the Hartmann–Shack sensor in the human eye. J Opt Soc Am A 2000;17:1388–1398.

7.- Moreno-Barriuso E, Navarro R. Laser ray tracing versus Hartmann-Shack sensor for measuring optical aberrations in the human eye. J Opt Soc Am A 2000;17:974-985.

8.- Davies N, Diaz-Santana L, Lara-Saucedo D. Repeatability of ocular wavefront measurement. Optom Vis Sci 2003;80:142–150.

9.- Salmon TO, Thibos LN, Bradley A. Comparison of the eye's wave-front aberration measured psychophysically and with the Shack-Hartmann wavefront sensor. J Opt Soc Am A 1998;15:2457-2465.

10.- Moreno-Barriuso E, Marcos S, Navarro R, Burns SA. Comparing laser ray tracing, the spatially resolved refractometer, and the Hartmann-Shack sensor to measure the ocular wave aberration. Optom Vis Sci 2001;78:152-156.

11.- Rodríguez P, Navarro R, González L, Hernández JL. Accuracy and reproducibility of Zywave, Tracey and experimental aberrometers. J Refract Surg 2004;20:810-817.

12.- Tyson, RK. *Principles of Adaptive Optics*. 2nd ed. Boston: Academic Press; 1997.

13.- Artal P, Chen L, Fernández EJ, Singer B, Manzanera S, Williams DR. Neural compensation for the eye's optical aberrations. J Vis 2004;4:281-287.

14.- Lopez-Gil N, Howland HC, Howland B, Charman N, Applegate R. Generation of third-order spherical and coma aberrations by use of radially symmetrical fourth-order lenses. J Opt Soc Am A 1998;15:2563-2571.

15.- Guirao A, Williams DR, Cox IG. Effect of rotation and translation on the expected benefit of an ideal method to correct the eye's higher-order aberrations. J Opt Soc Am A 2001;18:1003-1015.

16.- Andersson H, Ekberg M, Hard S, Jacobsson S, Larsson M, Nilsson T. Single photomask, multilevel kinoforms in quartz and photoresist: manufacture and evaluation. Appl Opt 1990;29:4259-4267.

17.- Suleski TJ, O'Shea DC. Gray-scale masks for diffractive-optics fabrication: I. Commercial slide imagers. Appl Opt 1995;34:7507-7517.

18.- Navarro R, Moreno-Barriuso E, Bará S, Mancebo T. Phase plates for wave-aberration compensation in the human eye. Opt Lett 2000;25:236-238.

19.- Bará S, Mancebo T, Moreno-Barriuso E. Positioning tolerances for phase plates compensating aberrations of the human eye. App Opt 2000;39:3413-3420.

20.- Liang J, Williams DR. Aberrations and retinal image quality of the normal human eye. J Opt Soc Am A 1997;14:2873-2883.

21.- Thibos LN, Applegate RA, Schwiegerling JT, Webb R. Standards for Reporting the Optical Aberrations of Eyes. Lakshminarayanan V, ed. Vision Science and Its Applications, vol. TOPS-35. Washington DC: Optical Society of America; 2000:232-244.

22.- Navarro R, Moreno-Barriuso E. Laser ray-tracing method for optical testing. Opt Lett 1999;24:951-953.

23.- Wang Z, Han B. Advanced iterative algorithm for phase extraction of randomly phase-shifted interferograms. Opt Lett 2004;29:1671-1673.

FIGURE CAPTIONS

Figure 1. – The calibration set. The nominal aberration generated by each plate is shown as both a wavefront aberration map (top) and its theoretical interferogram (bottom). Upper row: subset containing samples of different Zernike orders. Lower row: comatic subset with different amounts of the same mode.

Figure 2. – Experimental point-spread functions (PSFs). From left to right, PSFs corresponding to plates Z_5^{-1}, Z_6^2, Z_7^5, and Z_3^1 (4).

Figure 3. – Results obtained for the complete calibration set. First column (MZ), experimental Mach-Zehnder raw interferograms. Second column (LS), non-linear least squares fitting of the raw interferograms. Third column (HS), single-pass Hartmann-Shack wavefront sensor measurements. Fourth column (LRT), results with the ocular laser ray tracing aberrometer.

Figure 4. – Summary of results. Upper panel (a), RMS values for the nominal mode of each plate: design target values (white bars), measured with M-Z interferometer (grey), with H-S wavefront sensor (black), and two artificial eye measurements with biased and unbiased LRT (patterned bars). Lower panel (b), residual RMS wavefront aberration for the aberrometric measurements: H-S (black bars) and LRT (patterned) respectively.

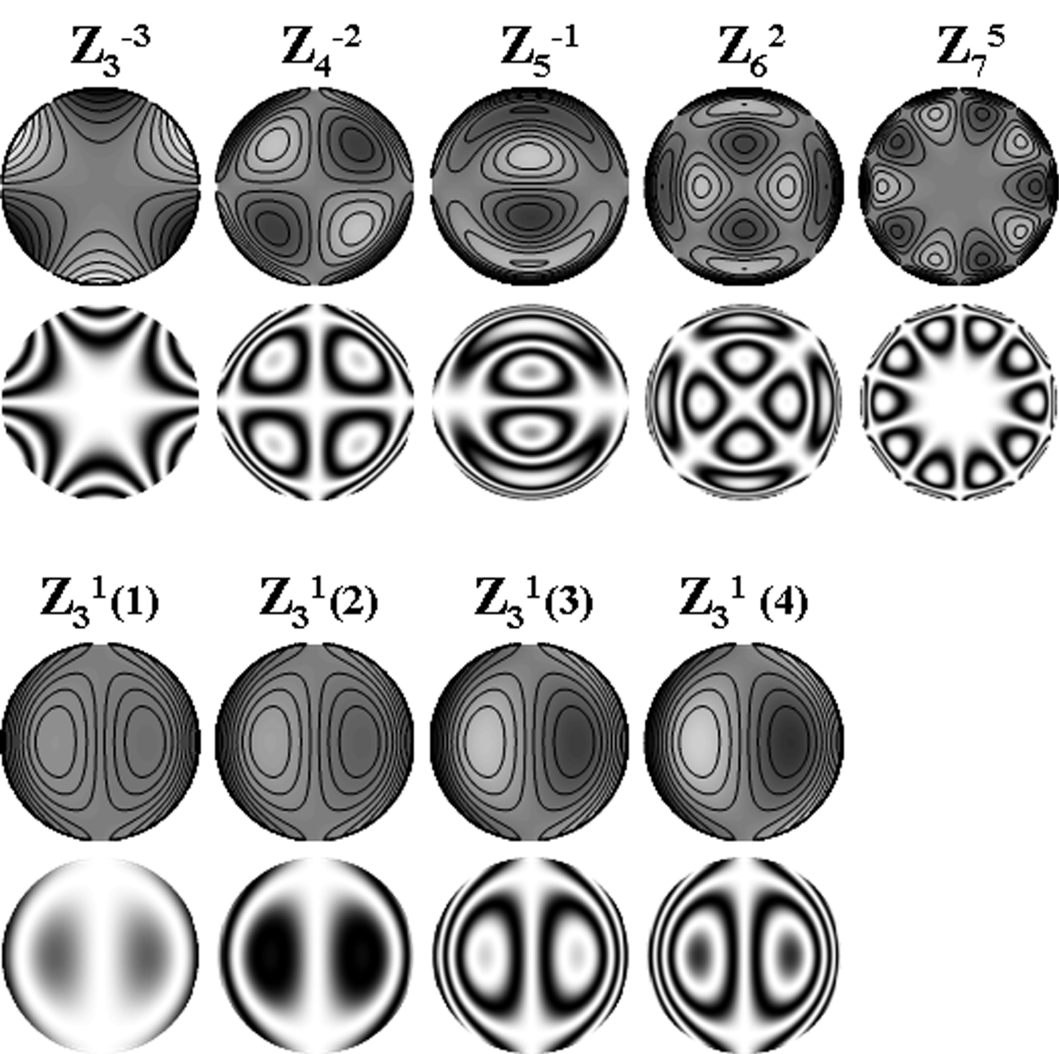
Z_3^{-3}
Z_4^{-2}
Z_5^{-1}
Z_6^{2}
Z_7^{5}
$Z_3^{1}(1)$
$Z_3^{1}(2)$
$Z_3^{1}(3)$
$Z_3^{1}(4)$

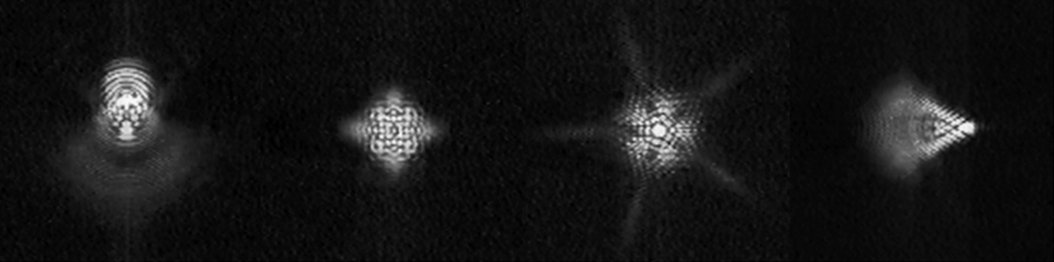

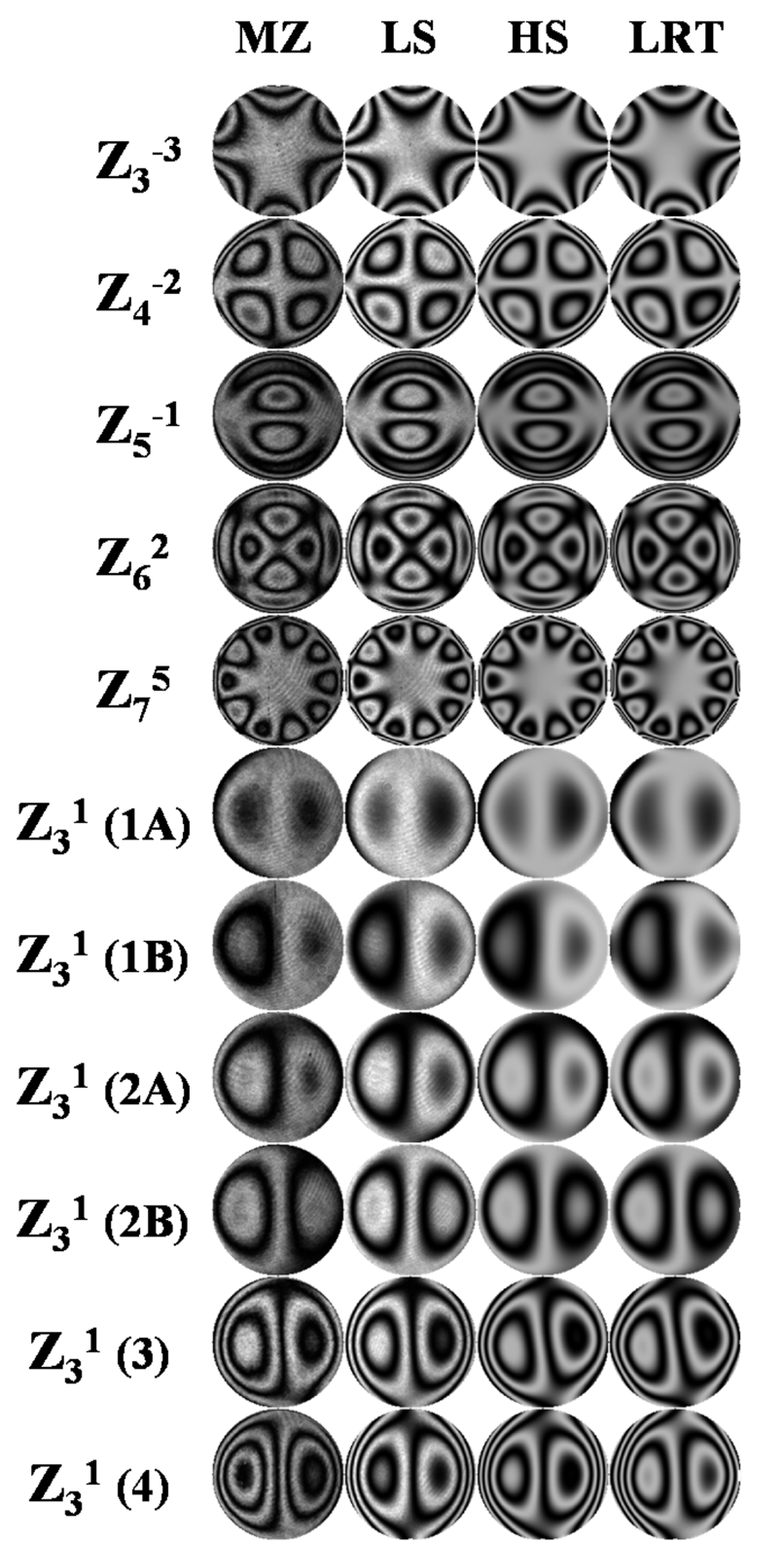
MZ
LS
HS
LRT
Z_3^{-3}
Z_4^{-2}
Z_5^{-1}
Z_6^{2}
Z_7^{5}
Z_3^{1} (1A)
Z_3^{1} (1B)
Z_3^{1} (2A)
Z_3^{1} (2B)
Z_3^{1} (3)
Z_3^{1} (4)

(a) RMS Nominal Mode

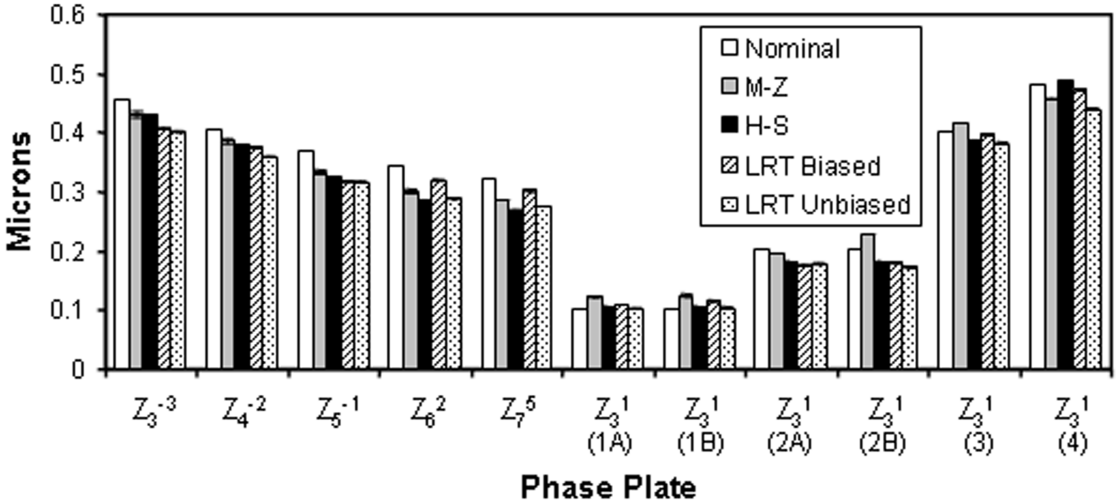

(b) RMS Residual Aberrations